Defect states of complexes involving a vacancy on the boron site in boronitrene

T. B. Ngwenya, A. M. Ukpong,* and N. Chetty

Department of Physics, University of Pretoria, Pretoria 0001, South Africa

(Dated: April 21, 2011)

Abstract

First principles calculations have been performed to investigate the ground state properties of free-standing monolayer hexagonal boronitrene (*h*-BN). We have considered monolayers that contain native point defects and their complexes, which form when the point defects bind with the boron vacancy on the nearest neighbour position. The changes in the electronic structure are analysed to show the extent of localization of the defect-induced mid-gap states. The variations in formation energies suggest that defective *h*-BN monolayers that contain carbon substitutional impurities are the most stable structures irrespective of the changes in growth conditions. The high energies of formation of the boron vacancy complexes suggest that they are less stable, and their creation by ion bombardment would require high energy ions compared to point defects. Using the relative positions of the derived mid-gap levels for the double vacancy complex, it is shown that the quasi donor-acceptor pair interpretation of optical transitions is consistent with stimulated transitions between electron–hole states in boronitrene.

PACS numbers: 71.15.Nc, 71.55.Ht, 73.22.Pr

*aniekan.ukpong@up.ac.za

I. INTRODUCTION

When graphene[1–3] was discovered in 2004 it was only a year before boronitrene (BN), which forms in the same honeycomb structure, was synthesised.[4] This mimicked, to a large extent, the initial prediction and subsequent discovery of cubic boronitride[5] with hardness comparable to diamond. Graphene has been the subject of intense investigations because of its unique properties, which makes it an attractive material for nano-scale electronic applications. Boronitrene is also gaining much attention these days because of the similarities with graphene, and the promising possibilities of unique properties for technological applications. The structural stability of these materials as free-standing layers has presented a remarkable opportunity for exploration of their properties for use in novel technological applications. This has given rise to a large number of model calculations of these unique materials.

The calculated 2D elastic modulus of boronitrene is ~40 Pa smaller than that of graphene.[6] Experimental measurements also confirm that boronitrene is softer than graphene.[7] Boronitrene is a direct band gap (5.5 eV) material,[7] and is found to be completely transparent in the ultraviolet (UV) - visible light range. Unlike graphene, which is a conductor, pristine boronitrene is an insulating material. The lattice parameter of boronitrene (2.50 Å) is so close to that of graphene (2.46 Å) that if the two materials were to form a composite, with one of them acting as the template, there would be essentially no lattice mismatch between them.[8] Boronitrene was predicted to be a very good substrate for graphene as it induces a band gap of 53 meV in graphene,[9] which makes this arrangement the best candidate for graphene-based microelectronics applications.[8]

Boron nitride nanotubes (BNNTs) exhibit impressive chemical stability, superior mechanical properties, and high thermal conductivity. By extension, there is a high possibility that a monatomic layer of hexagonal boronitrene will have similar properties.[10] The special combination of properties in boronitrene makes it a good substitute material for graphene in applications such as optoelectronic nano-devices, functional composites, hydrogen accumulators and dielectric substrates. The relatively fewer number of experimental studies on BN nanosheets indicates that two-dimensional BN is still yet to be fully explored, compared to graphene. This situation arises from the fact that the synthesis of BN-based nanostructures is more challenging than that of C-based nanostructures,[10] because the well-developed methods for graphene synthesis are not as suitable for boronitrene.

The creation of a variety of defects in BN has been shown to influence the electronic properties of the material significantly. First principles calculations[11] have shown that boronitrene

undergoes an insulator-semiconductor transition in the presence of structural defects. For instance, the replacement of a boron atom by a carbon impurity (C_B) was found to give rise to the smallest band gap. Such results predict the possibility of transforming the insulating boronitrene layer to a semiconducting layer by introduction of defects. In an experimental study, Jin *et al.*[12] found the boron vacancy to be energetically preferred to the nitrogen vacancy in boronitrene. In contrast, Azevedo *et al.*[13] found the nitrogen vacancy to be preferred in their computational study. Clearly, more studies – both experimental and theoretical, of boronitrene are needed. This paper focuses on the defect complexes formed through the binding of a native defect with the boron vacancy on nearest neighbour positions. Various defect configurations that form a first nearest neighbour with the boron vacancy have been considered.

II. METHODOLOGY

All the first principles calculations were carried out based on density functional theory as implemented in the Vienna *ab initio* Simulation Package (VASP).[14–17] The exchange-correlation potential was described in the generalized gradient approximation, as parameterized by Perdew, Burke, and Ernzerhof (PBE).[18,19] We also employed the quasi-particle (GW) approximation[20,21] to determine the optical absorption spectra of boronitrene. The VASP implementation is based on the projector-augmented wave method (PAW).[22.23] Our calculations were performed using a kinetic energy cut-off of 500 eV for the plane wave expansion and the total energy was converged to within 10^{-7} eV. The Monkhorst-Pack scheme[24] was used to sample the Brillouin zone. We tested the convergence of our results for total energy differences and structural parameters on the (1×1) conventional 2D cell, and we concluded that the (10×10×1) sampling of the Brillouin zone is sufficiently converged. For all subsequent calculations, we used a Monkhorst-Pack grid of density comparable to the (10×10×1) k-mesh applied to the (1×1) conventional cell. We used a periodic supercell geometry that exploits the plane wave formulation of the electronic structure problem. The separation for the boronitrene layers in the supercell was set at 15 Å, to avoid spurious interlayer interactions.

The total energy was also converged with respect to the supercell size in the defect calculations. The difference, δ_1 = -26.4758 eV, between the total energies of the 49 bonded B-N pairs in a (7×7) supercell of pristine *h*-BN and the most extended open-volume defective system is calculated as $49E_{\text{pair}}^{\text{BN}} - E_{7\times7}(\text{V}_\text{B} + \text{V}_\text{N})$. For the (5×5) supercell, the difference, δ_2 = -26.4764 eV, between the 25 bonded B-N pairs in the pristine, and V_B+V_N configuration is calculated as $25E_{\text{pair}}^{\text{BN}} - E_{5\times5}(\text{V}_\text{B} + \text{V}_\text{N})$. The difference ($\delta_1$-$\delta_2$) converges to 8 meV for the V_B+V_N complex.

Since the V_B+V_N configuration corresponds to the most extended open-volume defect, we used the (5×5) supercell in all the calculations reported here. Structural models of the possible defect geometries, which result from the binding between a point defect and the boron vacancy on nearest-neighbor positions, were constructed in each case, for the (5×5) supercell, such that the lattice parameter is always 12.55 Å. The electronic states were populated in accordance with the Fermi distribution function, with a Fermi smearing parameter of 0.2 eV. The atomic forces were calculated using the Hellman-Feynman theorem, and the atomic positions were relaxed until the forces were reduced to less than 0.01 eVÅ^{-1}.

III. RESULTS AND DISCUSSION

A. Structural properties

The total energy of the pristine layer was optimized with respect to the lattice parameter. The minimum-energy structure showed a lattice parameter of 2.51 Å for the hexagonal lattice. This compares favourably with the experimental value of 2.50 Å,[8,25,26] and with published results of other calculations.[11,27] In addition, the cohesive energy of the pristine layer was calculated using the expression

$$E_c = E_{\text{pair}}^{\text{BN}} - E^B - E^N, \qquad (1)$$

where $E_{\text{pair}}^{\text{BN}}$ is the total energy per pair of B-N atoms in the equilibrium structure. The terms E^B and E^N denote the total energies of the free B and N atoms respectively. The cohesive energy of -20.01 eV was obtained for the pristine 2D BN structure indicating its stability as a free-standing monolayer. The structure optimisation presented above gives an indication of the stability of the free-standing boronitrene monolayer. The relaxed configuration shows that the B-N bond length is 1.451 Å in the pristine monolayer. The optimised geometry of the V_N, V_B, V_B+C_N, N_B, B_N, V_B+V_N, C_B, C_N, and V_B+B_N defects in monolayer boronitrene are shown in Fig. 1 along with the interatomic distances in the neighbourhood of the defect centre.

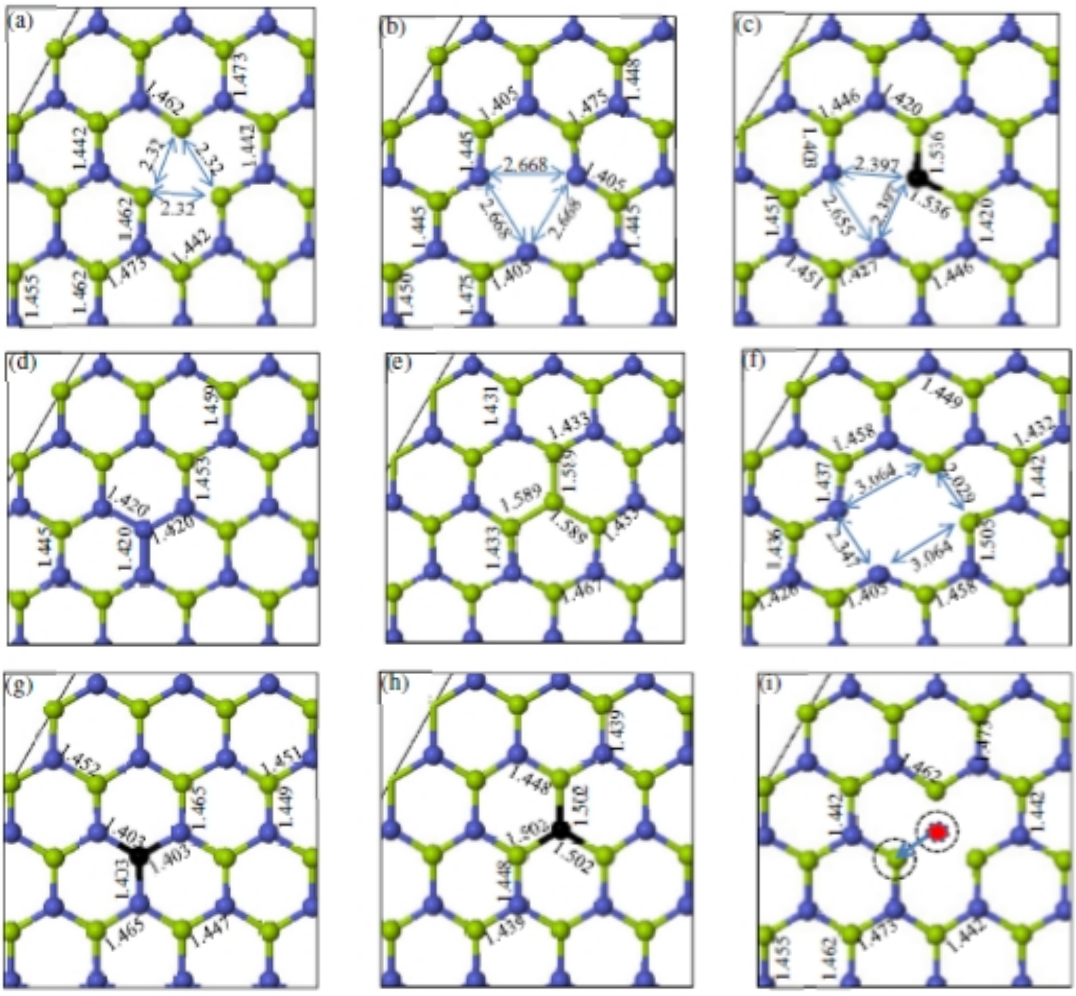

FIG. 1. The structural geometry of defective BN monolayers containing: (a) V_N; (b) V_B; (c) V_B+C_N; (d) N_B; (e) B_N; (f) V_B+V_N; (g) C_B; (h) C_N; and (i) V_B+B_N. The distortions of the local structure due to the defects are indicated (in Angstroms) as changes in interatomic distances relative to equivalent interatomic distances in pristine boronitrene, where equilibrium B-N bond length is 1.451 Å. The encircled ball at the defect centre denotes the position of the B-atom before relaxation. The encircled green ball denotes the B-atom after it migrated to the site of the missing N-atom.

The edges of the honeycomb structures buckle considerably after relaxation due to defects. Fig. 2 shows that the layers are atomically flat despite the observed *in-plane* structural changes. The mean B-N bond length and the strain in the defective layers relative to the relaxed pristine monolayer are presented in Table I. The B-N-B (and N-B-N) bond angles vary from the sp^2 hybridized bond angle of 120°, within the range $\Delta\theta = \pm 2.69°$, in each case. Since the average

change in B-N bond lengths is negative, except in the carbon-related defects, we conclude that the intrinsic point defects induce a compressive stress in the *h*-BN layer.

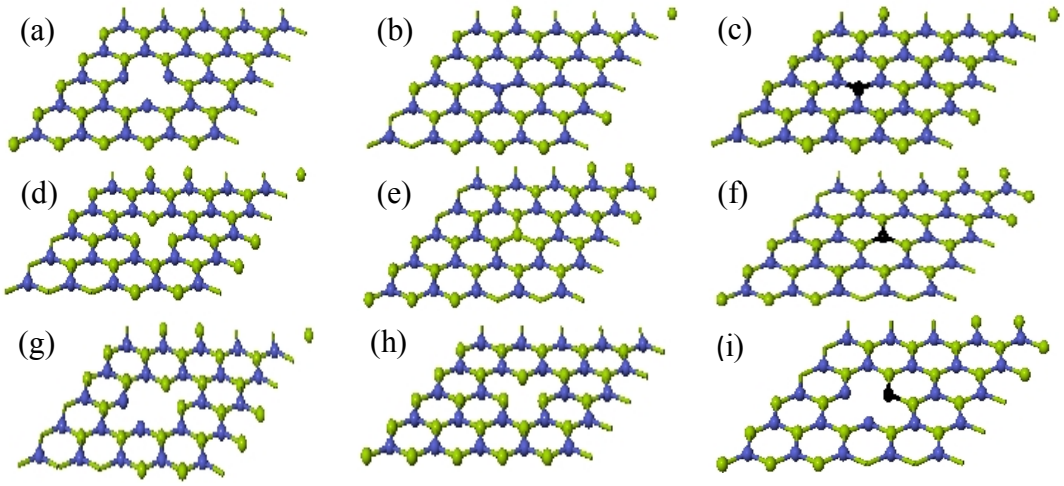

FIG. 2. Flat monolayers of hexagonal boronitrene showing buckled edges due to V_B (a); N_B (b); C_B (c); V_N (d); B_N (e); C_N (f); V_B+V_N (g); V_B+B_N (h); and V_B+C_N (i) defects after *in-plane* bond relaxations.

Table I. Mean bond length around defect centres in hexagonal boronitrene showing *in-plane* bond relaxations. The strain is evaluated as the percentage change in B-N bond length relative to the optimised bond length of 1.451 Å, where positive (+) or negative (-) strain denotes tension and compression, respectively.

	Structural properties	
Defect	$\langle l_{B\text{-}N} \rangle$ (Å)	Strain (%)
V_B	1.425	-1.792
V_N	1.447	-0.276
C_B	1.456	0.345
C_N	1.453	0.138
N_B	1.449	-0.138
B_N	1.450	-0.69×10^{-5}
V_B+V_N	1.445	-0.207
V_B+B_N	1.447	-0.276
V_B+C_N	1.452	0.414

Around the defects, there is a local reconstruction of the network structure. In the case of N_B and C_B antisite defects, the nearest neighbour atoms undergo a small inward relaxation leading to shorter B-N bonds, whereas in the B_N and C_N antisite defects there is a small outward breathing relaxation in near neighbour distances. In both cases, the hexagonal symmetry of the honeycomb structure is retained, thus maintaining the rotational symmetry about the axis normal to the defect centre. This 3-fold rotational symmetry is also conserved in vacancies for rotations about the site of the missing N or B atom. At the V_B defect centre, the three surrounding N-atoms draw electrons from the surrounding B-N bonds. As a result, the B-N bonds become shorter, and therefore stronger due to the inward breathing relaxation. The outward breathing relaxation in first neighbour N-B bonds is smaller in V_B than in V_N. Although the distances between the three non-bonded B-B (and N-N) in V_N (and V_B) are similar in each case, we also observe the small, symmetry-breaking, pseudo Jahn-Teller distortions in near-neighbour distances far away from the two defect centres. The reconstructions of the local structure are consistent with the results reported in Refs. 11, 13 and 28 for similar defects.

The 3-fold rotational symmetry of the pristine boronitrene monolayer is reduced to mirror symmetry when a double vacancy is created. The local structure of the V_B+V_N double vacancy complex imposes the mirror symmetry on the structure, about an axis through the open volume of the defect. An inspection of the B-N bonds attached to the 14-atom ring, which surrounds the vacancy open-volume, shows both inward and outward relaxations of interatomic distances. The changes in the near neighbour distances are consistent with the changes in local structure of the double vacancy reported by Attaccallite *et al.*[28] The single boron vacancy gives rise to a system that is deficient by three electrons. The simultaneous introduction of a B_N antisite further increases the electron deficiency to five. The unpaired electron in the V_B+B_N complex sets up an attractive potential well which traps the boron atom into a global minimum energy state. This causes the B-antisite atom of the complex to migrate to the original position of the missing N atom.

There is only one minimum energy path (MEP) for boron migration in the V_B+B_N complex due to the constraint imposed by the 2D hexagonal symmetry of the monolayer. This is indicated in Fig. 1(i) by the shortest distance between the two encircled atoms. We have investigated the boron migration along this MEP in terms of the changes in free energy of the transitional states between the initial V_B+B_N configuration and the final state in the structure reconstruction along the reaction path. The force projection (i.e. the nudged elastic band) method[29,30] was used to map the MEP within the transition state search module as implemented in VASP. This offers an effective method

of finding the MEP, since the initial and final states in the $V_B+B_N \rightarrow V_N$ transition are known. The migration energy barrier between the two equilibrium structures, i.e. V_B+B_N and V_N, were determined by optimising five images between the initial V_B+B_N structure and the final V_N structure along the reaction coordinate.

These five images are denoted by the five intermediate data points on free energy profile along the reaction path. The free energy landscape, in this case, is the distribution of the Helmholtz free energy of the $B_{25}N_{24}$ supercell in the harmonic approximation,[30] for which the spring constant that connects the atoms in adjacent images of the five transitional structures is set to 5.0 eV/Å^2. Transition states are only searched for the highest saddle point. The full structure optimization of the transition states is also carried out. The image closest to the saddle point is allowed to climb up into the saddle point when the largest force on an atom is smaller than 0.5 eV/Å using double nudging.[31] Fig. 3 shows the free energy profile of the V_B+B_N transitional states as a function of the B-B bond length for the $V_B+B_N \rightarrow V_N$ conversion. We find an activation energy of ~0.22 eV, and a potential barrier of 2.86 eV for the boron dynamics. The negative free energy along the reaction coordinate suggests that the boron migration is spontaneous at temperatures $T > 1703$ K (i.e. $T = 1703$ K corresponds to the thermal energy of 0.22 eV). At such high temperatures, the boron capture cross section should reduce due to its high momentum.

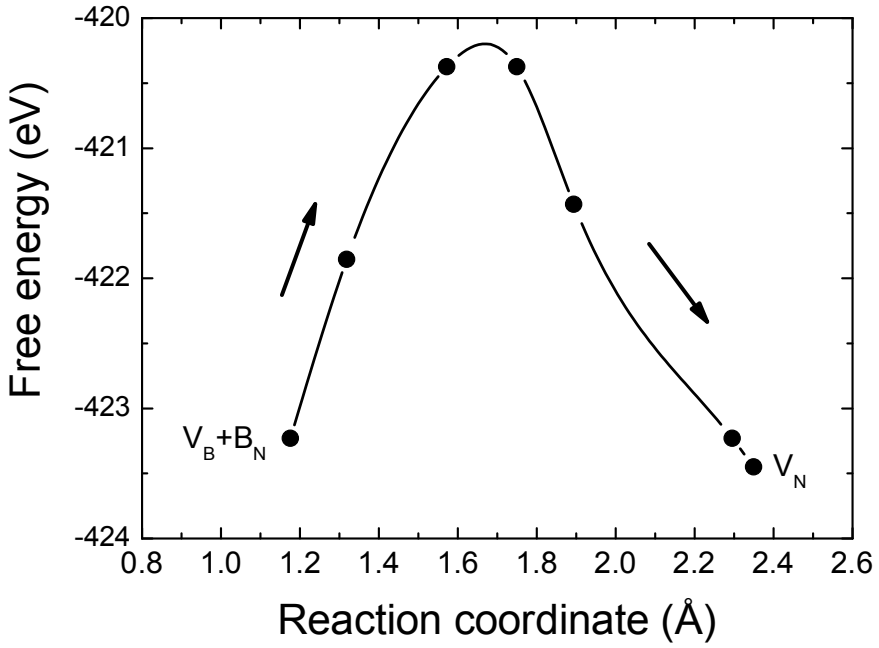

FIG. 3. Free energy profile for boron migration as a function of the B-B bond length in the V_B+B_N complex.

This boron migration imposes the 3-fold rotational symmetry of the V_N structure on the V_B+B_N complex. The structure of the V_B+C_B imposes the mirror symmetry about an axis bisecting the B-N-B bond angle normal to the position of the C-antisite. In the V_B+C_N complex, the distances between the two non-bonded C and N atoms are 2.397 Å. The equivalent distance of 2.668 Å in the V_B defect between two non-bonded N-N atoms is significantly longer. Hence, the relaxation of the surrounding B-N bonds in the V_B+C_N complex shows that C-substitution causes substantial distortions in the local structures which may influence the electronic properties.

B. Energetics

The formation energy of neutral point defects in the monolayer was calculated as a function of the changes in chemical potentials using the Zhang-Northrup formulation[32] for an arbitrary combination of atoms in the supercell as,

$$E_f(D) = E_{\text{total}}(D) - \sum_i n_i \mu_i , \qquad (2)$$

where $E_{total}(D)$ is the total energy of a supercell containing the defect of type *D*. The second term denotes the Gibbs free energy arising from the formation of n_i species of type *i* with chemical potential μ_i from B, N and C atoms, and bonded B-N pairs. Since the atomic chemical potentials are fixed by the condition $\mu_B + \mu_N = \mu_{BN}$ at thermodynamic equilibrium, it follows that the upper bounds for μ_B and μ_N correspond to the precipitation limits for formation of metallic boron and molecular nitrogen, in each case. This arises because the chemical potentials are constrained by the conditions $\mu_B \le \mu_B^{bulk}$ and $\mu_N \le \mu_N^{bulk}$ so that the formation energy of the defective monolayers are constrained to vary within the interval, $-\Delta H_f \le \Delta\mu \le \Delta H_f$, fixed by the heat of formation of pristine *h*-BN monolayer. We calculated the heat of formation of the pristine monolayer using $\Delta H_f = -(\mu_{BN} - \mu_B^{bulk} - \mu_N^{bulk})$ and obtained the value of -2.58 eV. This compares well with the experimental value of -2.60 ± 0.02 eV.[33]

Fig. 4 shows the formation energy of neutral defects $E_f^0(D)$ as a function of changes in atomic chemical potential $\Delta\mu$. The N-rich growth condition corresponds to the limit $\Delta\mu = -\Delta H_f$, in which the boron chemical potential, $\mu_B = \mu_{BN} - \mu_N$, is determined by the nitrogen chemical potential, so that the layer is in equilibrium with nitrogen gas (N_2). The B-rich condition, on the

other hand, corresponds to the limit $\Delta\mu = +\Delta H_f$, in which the nitrogen chemical potential, $\mu_N = \mu_{BN} - \mu_B$, is determined by the boron chemical potential, and the layer is in equilibrium with bulk metallic boron (α-B). The formation energy of non-stoichiometric defects depends strongly on the chemical potential, and therefore on the specific atomic reservoir employed in growing the *h*-BN monolayer. The creation of C-substitutional impurity at the B- and N- sites lead to substantially lower formation energies compared to the creation of either the N_B antisite, or the V_B defect. The V_N defect is generally more stable than the V_B defect in both conditions – as determined by the range of allowed variations in chemical potential. However, the V_B defect is relatively more stable in N-rich conditions than in B-rich while the V_N defect exhibits an opposing behaviour in both growth conditions. Similarly, the N_B antisite is more stable in the N-rich growth medium, while B_N antisite is more stable in B-rich condition.

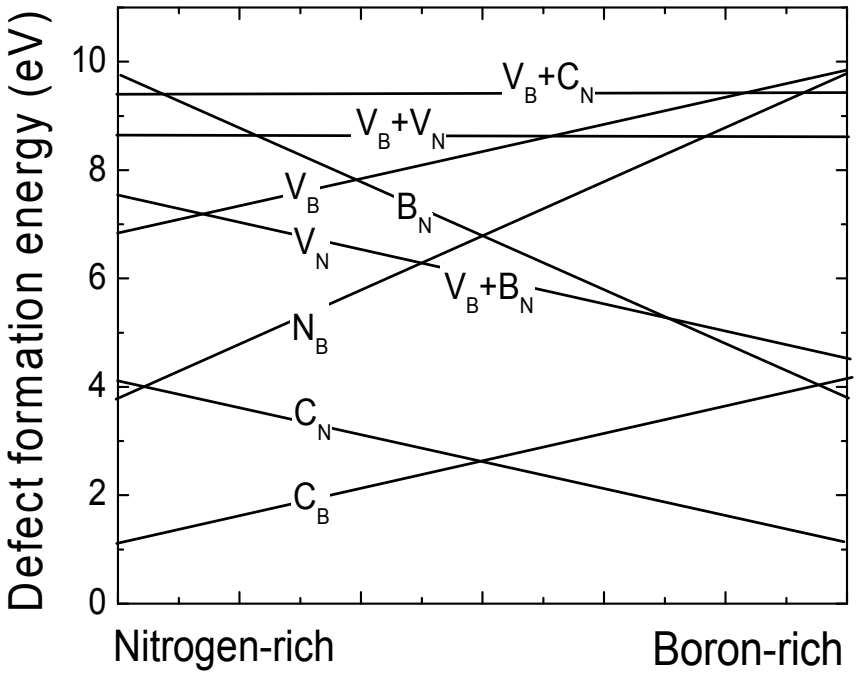

FIG. 4. Formation energy of neutral boron vacancy-related defects as a function of changes in chemical potential.

The relative stabilities of non-stoichiometric point defects in either B-rich (or N-rich) conditions indicate that defective configurations that induce an excess of either boron (or nitrogen) atoms in the *h*-BN monolayer are relatively more stable in the B-rich (or N-rich) atmosphere. This observation is consistent with *a priori* expectations for charge neutrality in equilibrium structures, and with the relative stabilities of neutral point defect in GaAs under Ga-rich and As-rich

conditions.[31] The low, non-negative, formation energies (see Fig. 4) means that although the defects do not form spontaneously in *h*-BN, it is possible to create them synthetically, possibly via low energy ion bombardment. This is consistent with experimental observations for nitrogen vacancies and interstitials created in *h*-BN after irradiation with N^{+2} ions.[34,35] The V_B+V_N and V_B+C_N complexes are stoichiometric defects. Their formation energies do not depend on the changes in chemical potential. The formation energy of the V_B+C_N complex (9.46 eV) is slightly higher than the formation energy of the double vacancy (V_B+V_N) complex (8.63 eV), hence, it is the least likely vacancy complex to form in typical *h*-BN monolayers.

The formation energy of the non-stoichiometric V_B+B_N complex is lower in B-rich conditions compared to the N-rich condition. The V_B+B_N and V_N defects present nearly the same formation energies across the range of allowed changes in chemical potential with differences less than 0.66 meV. This small difference in formation energy re-confirms the observed similarity in local structure of the two defects after reconstruction. Thus, there are two points in the chemical potential where the possibility of forming any one of three possible defects in *h*-BN is high (see Fig. 4). It is therefore equally possible to form any one of either B_N, V_N or V_B+B_N defects in B-rich growth condition, and any one of either B_N, V_B or V_B+B_N defects in the N-rich condition. Relatively low concentrations of stoichiometric boron vacancy complexes are expected in typical *h*-BN monolayers in both growth conditions because of their high formation energies. We conclude that it is energetically more favourable to form *h*-BN monolayers that contain a point defect than those that contains the vacancy complex. We therefore predict that C-substitutional impurities can bind favourably to the boron vacancy if the *h*-BN layer is bombarded with suitably energetic ions.

C. Electronic properties

1. Charge density distribution

Fig. 5 shows the contour map of plane-averaged difference charge density distributions along the normal to the plane of the monolayer as a superposition on the ball-and-stick representation of the corresponding structural model. For direct comparison, the contour plots denote the same isosurface value on the same scale. Fig. 5(a) shows the difference charge density distribution in the pristine structure. The B-N bonds show ionic character in all the cases considered. The extent of charge density localization along the B-N bond length is non-uniform. It is minimal at both B- and N- atomic centres, but progressively increases towards the bond centre with the global minimum localised at hollow sites. In the pristine ($B_{25}N_{25}$) structure, the charge density maximum is shifted towards the N atoms along the B-N bond length. This represents a net

transfer of charges from B to N atoms, and therefore gives the B-N bond its ionic character. Topsakal *et al*.[36] also observed that the difference charge density shifts towards the nitrogen atom along the B-N bond. We have ascribed this boron-to-nitrogen charge transfer in *h*-BN to the fact that nitrogen is more electronegative than boron by ~20 %.[37]

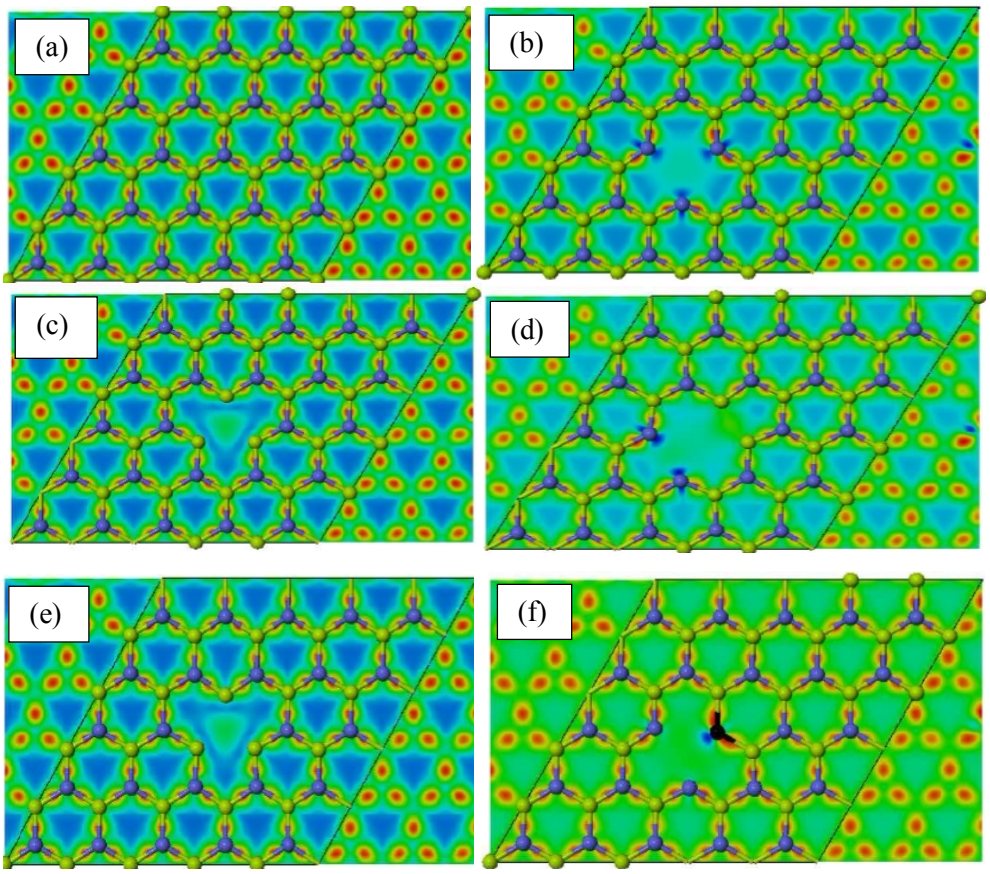

FIG. 5. Contour map of plane-averaged difference charge density distribution in the pristine layer (a); the isolated boron vacancy, V_B (b); the isolated nitrogen vacancy, V_N (c); the V_B+V_N complex (d); the V_B+B_N complex (e); and the V_B+C_N complex (f).

There is a symmetrical re-distribution of charges due to the missing boron and nitrogen ion cores (see Fig. 5(b) and (c)). However, the ionicity is locally enhanced along the B-N bonds, around the V_B defect compared to the V_N. The missing boron site results in a strongly localized minimum in difference charge density on each of the three N-sites surrounding the V_B defect. These sites can be interpreted as depletion zones for the positive charges. Relative to the V_B structure, the creation of an additional vacancy at the nitrogen site to form the V_B+V_N complex leads to significant redistribution of the charge density to hollow sites, and along the line joining the two non-bonded B atoms as seen in Fig. 5(d). In Fig. 5(e), we find a considerable reduction in

the charge density localisation along the B-N bond. This leads to a significantly reduced ionicity compared to the pristine structure. There is no net change in ionicity of the V_B+B_N complex relative to that of an isolated N vacancy.

The stoichiometric complexes have relatively higher formation energies compared to native defects (see Fig. 4). This suggests that re-distribution of charges due to the vacancy complexes is non-trivial in maintaining their energetic stability. A comparison of Figs. 1(b) and 1(c) suggests that the charge re-distribution in the V_B+C_N complex arises from the formation of the two long C-B bonds (1.54 Å) in V_B+C_N compared to the two short B-N bonds (1.41 Å) in V_B in an electron-deficient system. Hence, the resulting Jahn-Teller distortions preserve the V_B+C_N local structure at comparatively high energetic cost. The observed boron migration results in a global energy minimum and corresponds to the observed small differences between the formation energy of the V_B+B_N complex and the V_N defect. Fig. 5(d) shows that double vacancy (V_B+V_N) leads to the localized difference charge densities near the N-ends of the two B-N bonds on the two non-bonded N-atoms. In addition, although the two B-atoms around the open-volume of the defect are not bonded, there is evidence of charge transfer between them. This is due to the shortening of the B-B distance to 2.03 Å compared to the corresponding distance of 2.51 Å in the pristine structure. Fig. 5(f) shows that the introduction of a C-substitutional impurity at the N site near the boron vacancy causes charge transfer from the two surrounding B atoms to the C impurity. This leads to considerable redistribution of charges along the B-N bonds and also to hollow sites.

2. Electronic structure of the pristine *h*-BN monolayer

Boronitrene has the hexagonal symmetry of the 2D honeycomb structure similar to graphene, except that the number of valence electrons is 3 for B and 5 for N compared to 4 for C. Some of the valence band states of boron are degenerate unlike in nitrogen. The B *s* and *p* states overlap significantly with the N *s*- and *p*-states in the valence band, thus confirming that the covalent bonding in BN arises from sp^2 hybridization. In particular, the deep- and top- lying valence states are dominated by N *s* and *p* states respectively, since the relative contribution from B states to the valence band is less than 25 %. Figs. 6 (a) and 6(b) shows the band structure, and the density of states (DOS) for the pristine structure. In all the structures, the energy bands are aligned so that Fermi level corresponds to 0 eV, and the valence and conduction bands are well-separated by the band gap. Taking the Fermi level as reference, the energy gaps have been calculated as the energy difference between the valence band maximum (VBM) and the conduction band minimum (CBM). Apart from the boron vacancy complexes, for which no experimental study or other theoretical

calculations have been reported, there is a good agreement between our band gap estimates and other results for the point defects.

The general features of the energy bands agree with previous studies,[11,13,34] and confirm the semiconducting behaviour of the pristine boronitrene layer. At point K, the valence band maximum ε_v is located at -0.09 eV, just below the Fermi level. This highest occupied energy level is lowered to -0.31 eV at the Γ-point. When the position of the CBM is fixed at the Γ-point, a direct gap of 5.08 eV is obtained. An indirect gap of 4.87 eV is obtained for the Γ-M (or Γ-K) optical transition.[38] With the VBM fixed at point K, the calculated direct band gap is ~8% lower than the 5.5 eV determined experimentally.[7] The indirect band gap determined in the present GGA-PBE calculation is 2.7% higher than the 4.75 eV obtained in the first principles calculations of Azevedo *et al.*[11] The underestimated direct gap is attributable to the well-known drawbacks of the DFT method.[39-41]

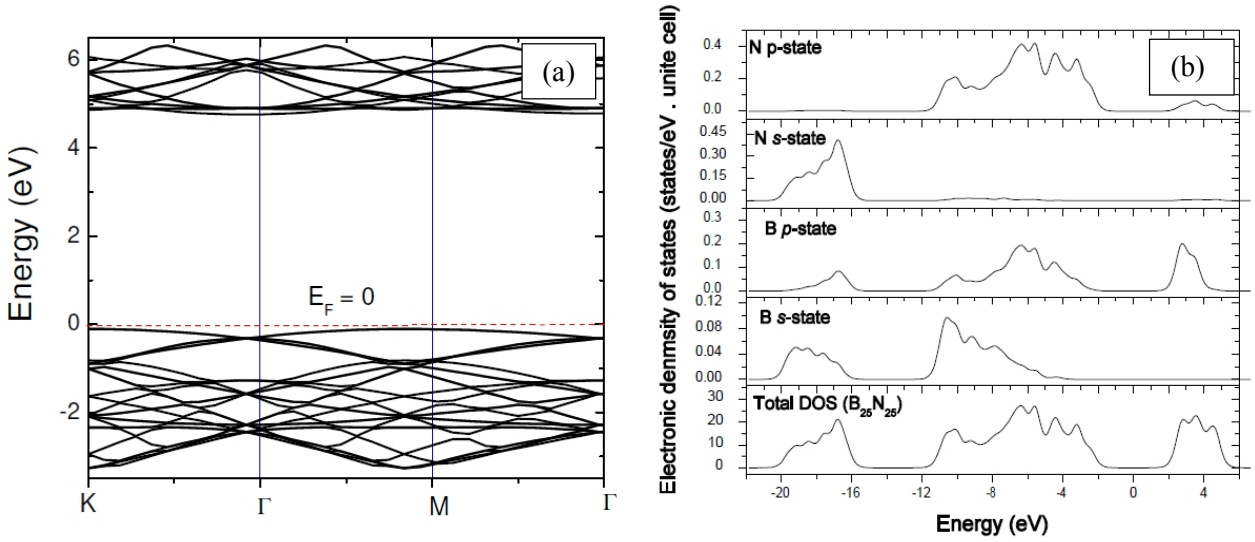

FIG. 6. Electronic band structure (a), and combined plots of total and orbital angular momentum-resolved total density of states (b) in pristine hexagonal boronitrene showing a wide gap between the top of the valence band and the entire conduction band.

Our GGA-PBE direct band gap is wider than the 4.82 eV predicted recently in LDA calculation for the *h*-BN monolayer.[28] The agreement between our GGA-PBE and the GW band structures is qualitative because although the $E(k)$ dependence on Brillouin zone direction is correctly predicted in both methods, subtle differences are observed in the band energies at high symmetry points. Table II shows the eigenvalues of the highest occupied molecular orbitals (HOMO) and lowest unoccupied molecular orbitals (LUMO) levels, in the pristine monolayer,

relative to the Femi level in the band structures calculated using the two methods. This shows that the quasi particle approximation consistently predicts lower (and higher) band energies for the HOMO (and LUMO) level at high symmetry points compared to GGA-PBE. The difference in the GW band energies at Γ-point yields a direct band gap of 6.03 eV. Although the GW band gap is more accurate than the LDA band gap, it is overestimates the experimental direct band gap by 9.63%. Due to the over-correction of the direct band gap, we have based our discussion of defect-induced single-particle energies on the indirect band gap determined from GGA-PBE calculations.

Table II. HOMO and LUMO levels in pristine hexagonal boronitrene monolayer relative to the Femi level (E=0 eV) at high symmetry points from GGA-PBE and quasi particle (GW) methods.

Electron State	Approximation	Eigenvalues (eV)		
		Γ	M	K
HOMO	GGA-PBE	-0.31	-0.10	-0.09
	GW	-0.95	-0.56	-2.14
LUMO	GGA-PBE	4.77	4.49	7.22
	GW	5.08	4.83	7.46

3. Defect states

Defects play significant roles in determining the physical properties of materials. By extension, the properties of free-standing one-atom thick layers of *h*-BN are also expected to be influenced by defects. Structural defects may be introduced deliberately during synthesis, but can also occur spontaneously due to the thermodynamic constraints imposed by the growth conditions. In the following section, we discuss the defect-induced one-electron levels derived from GGA-PBE band structure, and identify donor and acceptor levels. We also discuss the calculated mid-gap defect states within the context of experimentally determined optoelectronic properties of typical *h*-BN materials.

3.1 Vacancies

The introduction of a single boron vacancy means that there is one less B *s*-state in the valence band, and the total number of electrons in the system is reduced by three. The three dangling bonds on the surrounding nitrogen atoms should create three defect states. Nevertheless, the electronic properties of the vacancy-induced states correspond to the a_1 (one-state) and t_2 (two-state) irreducible representation of the T_d point symmetry group. The band structure shows two defect-related levels in the band gap region. Firstly, we find an unoccupied, non-dispersive

LUMO-level defect at the bottom of the conduction band. The unoccupied defect level is localized at ε_v+0.18 eV within the band gap. At the Γ-point, the energy of this defect state is 85 meV relative to the Fermi level. This defect state lies on the top of the valence band, and splits-off into half-filled level with energy ε_v+0.065 eV along the Γ→M and Γ→K directions at K. Indeed, this HOMO defect level forms an *s*-like resonance with the top of the valence band.

Analysis of the GGA-PBE one-electron energies shows that the half-filled dispersive defect state is a degenerate *p*-like t_2 state (HOMO-level), consistent with the triple acceptor role of the boron vacancy.[42-44] The DOS shows significant perturbation of the B and N *p*-states due to the V_B defect. This perturbation results in an upward shift in the valence band maximum and gives the V_B-induced defect states an overall *p*-like character. The small energy width for the HOMO-LUMO split-off suggests that the inward breathing relaxation seen in B-N bonds around the V_B defect is consistent with a small symmetry lowering Jahn-Teller distortion necessary to realize the lowest-energy state and preserve the hexagonal symmetry.[44]

For the nitrogen vacancy, we find at partially occupied HOMO defect state at ε_v+0.12 eV in the band gap region. More importantly, the number of conduction band states significantly increases compared to the pristine structure. Following the descriptions of Rak *et al*. for GaSe,[45] and GaTe,[46] the band structure can be interpreted in terms of the bonding model in BN. The observed changes in band structure are described in terms of simultaneous formation of bonding and anti-bonding states by B-B dimers. In *h*-BN, the hybridization between the B *s* and N *p* states tend to cause some of energy bands to shift upwards into the region of high energy, thus creating the observed wide semiconducting gap. The LUMO defect level (a_1 state) is observed at the ε_v+1.70 eV at bottom of the conduction band. At the Γ-point this defect state is non-dispersive and non-degenerate. This lowest unoccupied (a_1) defect energy level becomes strongly dispersive along the Γ→K and Γ→M directions with a maximum split of ~0.081eV at the K and M point of the BZ.

In the free-standing boronitrene layer considered here, the observed split off energy is small. For a rolled boronitrene layer however, Schmidt *et al*.[47] found a larger exchange splitting of 0.5 eV. Another nearly non-dispersive defect state is localised at the top of the valence band. We have examined this defect band closely, and found that it is half-filled, forming an *s*-like resonance with the Fermi level (E = 0). From the orbital angular momentum resolved density of states, we conclude that the mid-gap defect bands originate from the *p*-states of the three B atoms, which surround the N vacancy.

Before comparing our findings for the V_N defect with other similar calculations, it is worthy to note that Orellana and Chacham[44,48] reported a fully occupied *s*-like a_1 state in the band gap close to the valence band edge for bulk cubic boron nitride (3D *c*-BN). They also found a doublet, which splits into two singlets, lying as an *e*-resonance to the bottom of the conduction band. Our result for the *h*-BN monolayer confirms the presence of the *s*-like resonance level at the bottom of the conduction band. However, being a conduction band state, ours is half-filled. We cannot classify the neutral nitrogen vacancy as unstable as suggested in Ref. 44 because of its low formation energy. Thus, the unpaired electron in the HOMO level should be readily promoted to a higher energy level, thus making the V_N defect to assume the donor role.

3.2 Antisites

The introduction of a single B_N antisite gives rise to a deficit of two electrons in the system. The B atom binds strongly to the three surrounding B atoms to maintain the 3-fold rotational symmetry of the hexagonal structure. From the band structure, it is found that the B_N antisite introduces three defects levels into the band gap. We find two fully-occupied levels at the top of the valence band and one unoccupied level at the bottom of the conduction band. The two valence band levels at ε_v+0.94 eV and ε_v+0.71 eV are fully-occupied. The ε_v+0.71 eV defect state is strongly dispersive and degenerate. The third defect level is located at the bottom of the conduction band. This unoccupied LUMO defect level is located at ε_v+1.35 eV deep inside the band gap. The HOMO-LUMO barrier is 0.41 eV, and indicates the amount of work necessary to free an electron from the potential well.

On the other hand, the introduction of a single N_B antisite gives rise to a surplus of two electrons in the system. The N_B antisite also introduces three defects levels – two unoccupied states and one fully-occupied state into the band gap. For the N_B defect, the fully occupied defect-induced level is found at ε_v-0.06 eV, just outside the band gap region, below the valence band maximum. This HOMO defect state, which forms *s*-like resonance with the conduction band, is considered to originate from the large energy split between the a_1 level and the next lower energy valence band state. Within the band gap, there are two closely spaced unoccupied defect levels at ε_v+2.24 eV and ε_v+2.29 eV near the bottom of the conduction band. The energy difference between the LUMO level and the next unoccupied higher-energy level is 2.38 eV. This is an indication of the work that must be done in extracting the electron from a layer containing the N_B defect. In summary, electron rich (or deficient) defective systems are observed to introduce hole (or electron) states and thus have reverse donor (acceptor) roles respectively.

3.3 Carbon substitutional impurities

The introduction of a C-substitutional impurity on the B site to form the C_B defect gives rise to an extra electron in the system. Similar to the case of B_N and N_B antisites, the symmetry lowering distortions of B-N bonds around the C_B defect has a non-negligible influence on the band structure. The electronic structure changes to favour clear roles of electron donor/acceptor. The highest occupied defect level (ε_v+0.12 eV) appears to form as a split-off from the conduction band. The difference between this HOMO defect level and the next higher energy state in the conduction band (ε_v+0.98 eV) is 0.86 eV. This energy is small compared to the ~4.0 eV difference between the HOMO level and the next fully filled state in the valence band (ε_v+4.09 eV). Similar to the N_B antisite, there is a high energy difference between the two topmost occupied defect levels. In contrast to the C_B defect, the C-substitutional impurity on the N site (i.e. C_N antisite) gives rise to a deficit of one electron in the system. The LUMO level for the C_B defect is located at ε_v+1.07 eV. For the C_N defect, there is a partially-filled defect level in the band gap at ε_v+0.07 eV, which appears to have split from the valence band. In addition, an unoccupied LUMO defect level is found at ε_v+4.12 eV.

3.4 Boron vacancy complexes

Fig. 7 shows the DOS spectra of the boron vacancy complexes. In the double vacancy (V_B+V_N) the total number of electrons reduces by eight, hence the resulting system has zero total spin. Thus all valence band states are expected to be fully occupied. We find the presence of two doubly-occupied, nearly degenerate defect levels at the top of the valence band in the band structure. The two defect levels are located at ε_v+0.88 eV and (ε_v+0.90 eV) within the band gap. In addition, we find two unoccupied defect levels at the bottom of the conduction band. These two unoccupied levels are located at ε_v+0.84 eV and ε_v+3.68 eV within the band gap. The defect states observed in the valence band region come from the *p*-states of nitrogen, while the two defect levels in the bottom of the conduction band are from the *p*-sates of boron. The strong inward relaxation of B-N bonds around the centroid of the V_B+V_N double vacancy lowers the LUMO level to 0.78 eV. This reduces the energy gap to 0.80 eV. At point K, two fully-occupied *p*-like defect levels are found at energies -0.11 and -0.23 eV. It must be noted that these two occupied levels cannot be ascribed to the defect complex because they do not occur in the band gap region.

Nevertheless, as we move away from the point K, in the directions Γ→K and Γ→M, the two splits levels become degenerate. Within the band gap, the two unoccupied defect levels at the

bottom of the conduction band suggest that the V_B+V_N complex would readily act as acceptor of electrons promoted from the valence band through controlled doping or photon excitation. For the V_B+C_N complex, a partially-occupied non-degenerate HOMO defect level is found at the Γ-point. This is located just above the valence band at ε_v+0.13 eV. Also, an unoccupied defect level is obtained at ε_v+1.56 eV. This HOMO level corresponds to the -0.03 eV level at K, and lies just below the Fermi level, while the LUMO level is located at 1.44 eV. The energy gap of the V_B+C_N structure (1.44 eV) is 0.03 eV lower than the energy gap in V_N (or V_B+B_N). In addition, the singly-occupied electron states in C_N and C_B at the top of the valence band show that in substitutional doping with carbon, the C atom will always serve as a donor of electrons.

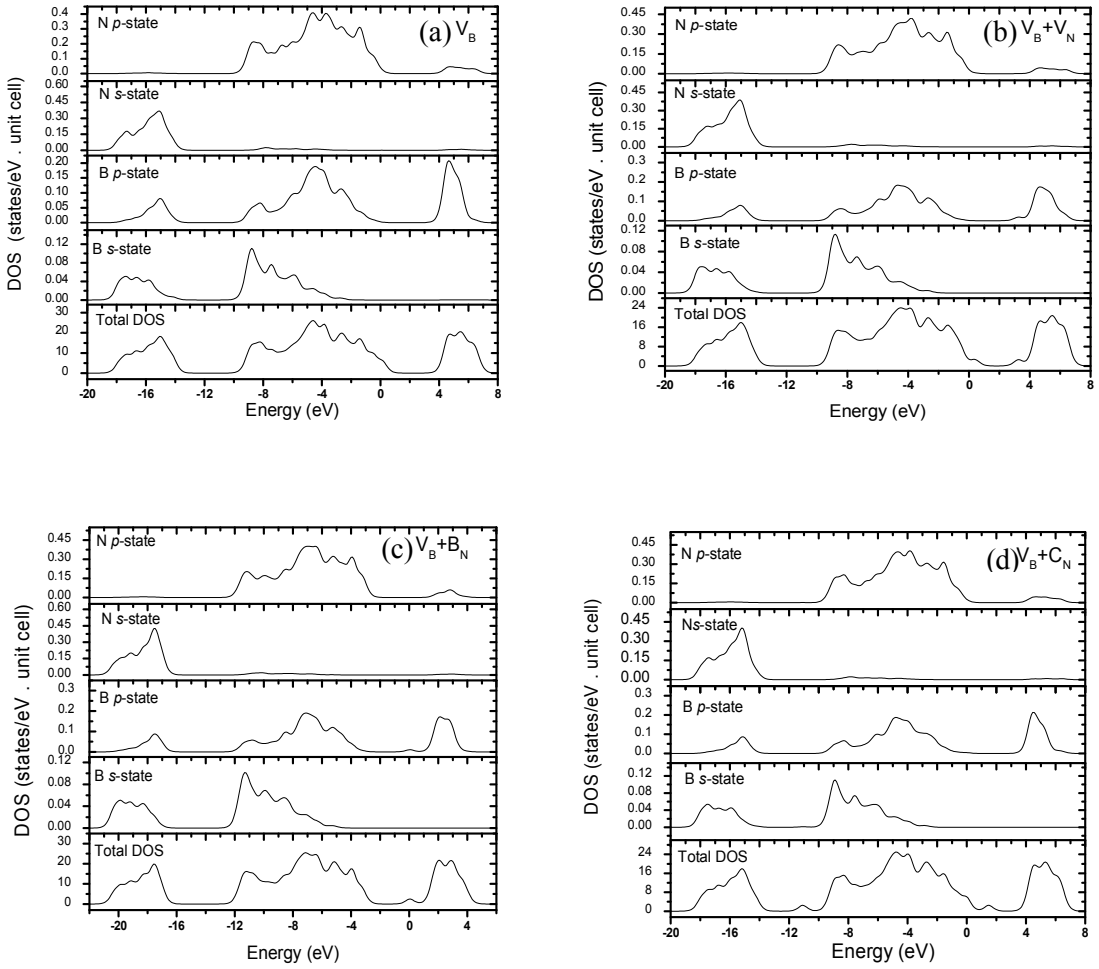

FIG. 7. Electronic density of states for defective boronitrene layers containing: V_B (a); V_B+V_N (b); V_B+B_N (c); and V_B+C_N (d); complexes.

4. Defect-induced optical transitions

All the defect-induced one-electron energy levels, shown in Fig. 8, were calculated relative to the valence band maximum in the pristine *h*-BN monolayer. The top of the energy gap corresponds to the conduction band minimum in the pristine layer. All the structural defects introduce localized energy level in the mid-gap region as expected. For V_B-related defects in particular, it is found that a small split-off energy (~1 meV) is sufficient to induce partially occupied *p*-like HOMO levels in the valence band. The main observation is that the origin of the dominant defect levels at the top of the valence band is traceable to *p*-like bonding states. These arise from nearest neighbour atoms of nitrogen (or boron) which surround the missing ion core when a boron (or nitrogen) vacancy is introduced. In particular, the defect-induced energy levels at the bottom of the conduction band are due to the B *p*-states.

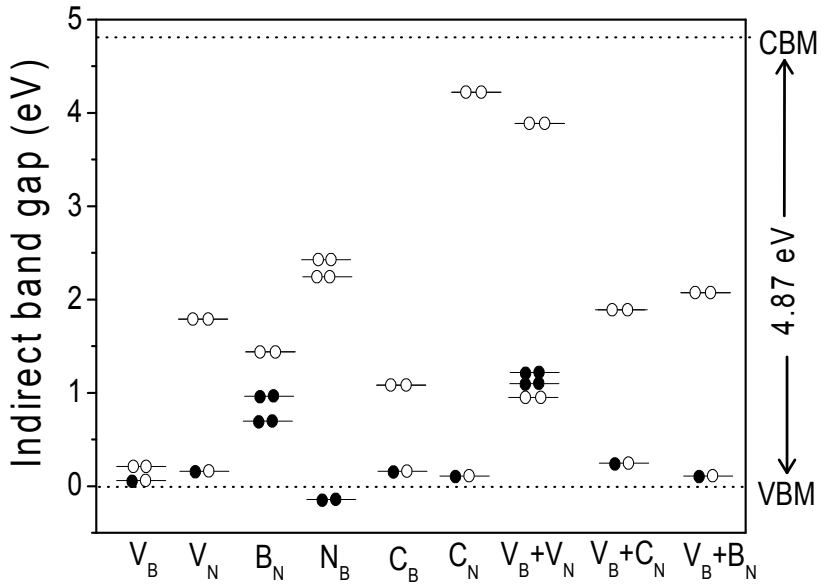

FIG. 8. Defect-induced one-electron energy levels derived from GGA-PBE band structures. The filled dots indicate electron states, while open dots denote hole states.

The electronic structure shows that boron vacancy complexes eliminate the wide band gap seen in the pristine *h*-BN monolayer due to band-crossing at the Fermi level. Our results establish the fact that the spontaneous presence of point defects or their complexes in atomically-thin BN materials or by doping them with carbon impurity modifies the band gap. This suggests that the constant-energy-gap observed in single-, and multi-walled BN nanotubes[49] can be systematically modified by incorporating point defects or by impurity doping. The split in the LUMO level of V_B-related defects in BN nanotubes,[47] at distances away from high-symmetry BZ points has been

attributed to an exchange-splitting effect due to paired electron spins. We have checked for this effect in the free-standing *h*-BN layer in spin-polarized calculation. The results do not change significantly from the previous spin-unpolarised calculation. It is therefore plausible that this effect could be related to the curvature of the nanotube.

One way of relating the results of experimental measurements of typical *h*-BN monolayers with theoretical predictions is to study the optical spectra. This is because photo-stimulated inter-band transition in *h*-BN materials is sensitive to the electronic structure.[50] The sub-structures[51-55] observed in the luminescence spectra of BN materials can therefore be explained in the context of optical inter-band transitions from electron-hole pairs. However, since density functional theory (DFT) is a ground state formulation, its standard approximations do not yield the correct excitation energies. On the other hand, the quasi-particle (GW) approximation gives a correction to the energies of single-particle excitation,[56] and can be used to simulate the photoemission spectrum. However, the simulation of optical transitions between two bands would require going beyond the GW approximation, to include the effect of the interaction between an electron in a higher band and the hole it left behind in the lower band. For the inter-band transitions, the Bethe-Salpeter equation correctly accounts for the interaction between electron-hole pairs in the excited state using the functional derivative of single-particle energies.[57,58]

In this analysis, we have assumed that the energies of the quasi particles in the photoemission spectrum of h-BN material are close to their ground state energies due to similarities between the quasi particle and GGA-PBE band energies in the pristine monolayer (see Table II). Fig. 9 shows the optical absorption spectra derived from GGA-PBE and G^0W^0 quasi-particle band structures for simulated photon excitation in an *h*-BN monolayer containing the V_B+V_N complex. There is a well-resolved absorption peak at 0.33 eV, and a slightly shifted absorption peak at ~1.5 eV (quasi-particle spectrum) and at ~ 2.1 eV (GGA-PBE), in addition to a broad absorption band between ~3.0 and ~9.0 eV. A direct comparison of the absorption spectra (Fig. 9) with the mid-gap defect levels of the V_B+V_N complex (Fig. 8) shows that the 0.33 eV absorption peak is not defect-related. Also, neither the 1.5 eV nor the 2.1 eV absorption peak positions match the ε_v+0.88 eV and ε_v+0.90 eV defect levels. However, the optical absorption spectra of the *h*-BN monolayer can be interpreted in terms of optical transitions from electron - hole states. Photo-stimulated electronic transitions from the nearly degenerate occupied levels to the empty LUMO level at ε_v+3.68 eV is consistent with the broad absorption band in Fig. 9. An alternative interpretation in terms of holes excitation from the unoccupied non-degenerate level around ~1 eV to the LUMO level is also a distinct possibility.[28]

The elusive nature of the four-peak deep-level emission band at ~4 eV,[51-55] and its observation in a broad class of BN materials - bulk polycrystalline *h*-BN,[51] BN nanotubes,[52-54] and *h*-BN powders[55] suggest that its origin is intrinsic to the honeycomb structure, and not a signature of the measurement conditions. Watanabe *et al*.[59] attributed this feature to electronic transitions from deep-level impurities based on luminescence measurements on high-purity *h*-BN single crystals. Since Zhang *et al*.[60] and Taylor II *et al*.[61] both wrongfully[55] attributed it to the band gap at ~4 eV,[53,62] the one-electron defect levels presented in this study have to be understood as the first step towards unravelling its origin. In the cathodoluminescence (CL) excitation spectrum of *h*-BN powder for instance, the 5.55 eV emission band shows three well-resolved sub-peaks at 5.35, 5.48, 5.76 eV, in addition to a fourth diffuse peak at 5.88 eV.[55] The photoluminescence (PL) spectrum, on the other hand, reveals two more sub-peaks at 5.56 and 5.64 eV at the same photon excitation energy, in addition to the four previous sub-peaks seen in the CL spectrum. Photoluminescence data is usually interpreted using the exciton-defect bound states model,[54,63] although alternative interpretations based on quasi donor-acceptor pairs,[64] exact hexagonal symmetry breaking due to defect,[65] and dynamic Jahn-Teller effect,[66] have also been reported. In spite of all these, the exact origin is still unclear. Although these same field emission characteristics have been interpreted recently in terms of the simultaneous co-existence of free and bound exciton-defect states,[28] the determination of their exact origin will require moving beyond the ground state to include excitonic effects on the defect states.

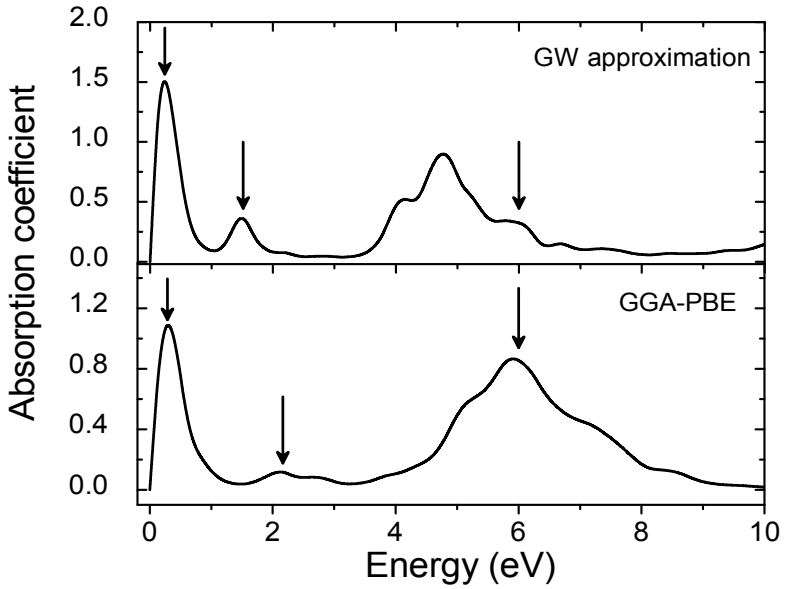

FIG. 9. The optical absorption spectra of a boronitrene layer which contains the V_B+V_N complex obtained using GGA-PBE (bottom panel) and G^0W^0 quasi-particle (top panel) approximations.

IV. CONCLUSION

In summary, we have performed first principles calculations to investigate the ground state electronic structure of boron vacancy complexes using the generalized gradient approximation of the density functional theory. We have addressed the question of the formation and relative stability of neutral defects that are associated with the boron vacancy site in boronitrene layers. It is found that the energies of formation of the boron vacancy complexes are generally higher than those of point defects. It is also observed that the V_B+B_N complex undergoes a spontaneous transformation to the V_N structure above 1703 K. The energetic stabilities show that non-stoichiometric point defects and vacancy complexes that induce excess nitrogen or excess boron atoms, in each case, are relatively more stable in the atmosphere corresponding to the excess species. The observed low formation energy of both V_N and V_B+B_N complex in B-rich condition is attributed to the excess boron in the layer. Thus, irrespective of the conditions of growth, formation of both defects is equally possible in the *h*-BN monolayer. The symmetry breaking Jahn-Teller distortions of the local structure due to electron deficiency in the V_B+C_N complex causes significant charge density fluctuations and results in relatively higher formation energy. We therefore conclude that decorating the boron vacancy with an antisite defect, a carbon substitutional impurity or the nitrogen vacancy on the nearest neighbour position does not enhance the structural stability of the resulting defect complex.

Furthermore, we have confirmed the acceptor/donor roles of electronic defects, and find that the trends for variation in energy band gap of *h*-BN monolayers due to defect incorporation is consistent with other calculations. We also find that all the HOMO levels at the top of the valence band are *p*-like states. Defect induced optical transitions from electron-hole pairs is suggested as the possible interpretation of the elusive features seen in luminescence spectra of typical BN materials. It is demonstrated that the sub-structures seen in photoluminescence excitation spectra of *h*-BN materials is consistent with the broad absorption band in the calculated optical spectra.

ACKNOWLEDGMENTS

We are grateful to Professor Angus Kirkland for helpful comments. TBN expresses gratitude to the National Institute for Theoretical Physics for financial support. AMU acknowledges financial support from the University of Pretoria under E2020 Project 5. NC thanks Professors Johan Malherbe and Max Braun for useful discussions. The authors are grateful to Professor Jannie Pretorius for assistance with the VASP code.

REFERENCES

[1]K. S. Novoselov, A. K. Geim, S.V. Morozov, D. Jiang, Y. Zhang, S. V. Dubonos, I. V. Grigorieva, and A. A. Firsov, Science **306**, 666 (2004).

[2]A. K. Geim, and K. S. Novoselov, Nature Mater. **6**, 183 (2007).

[3]K. S. Novoselov, A. K. Geim, S. V. Morozov, D. Jiang, Y. Zhang, M. I. Katnelson, S. V. Dubonos, I. V. Grigorieva, and A. A. Firsov, Nature **438**, 197 (2005).

[4]K. S. Novoselov, D. Jiang, F. Schedin, T. J. Booth, T. T. Khotkevich, S. V. Morozov, and A. K. Geim, Proc. Natl. Acad. Sci. **192**, 30 (2005).

[5]E. Knittle, R. M. Wentzcovitch, R. Jeanloz, and M. L Cohen, Nature **337**, 349 (1989).

[6]A. Nag, Kalyan Raidongia, K. P. S. S. Hembram, R. Datta, U. V. Waghmare, and C. N. R. Rao, ACSNANO **4**, 1539 (2010).

[7]L. Song, L. Ci, H. Lu, P. B. Sorokin, C. Jin, J. Ni, A. G. Kvashnin, D. G. Kvashnin, J. Lou, B. I. Yakobson, and P. M. Ajayan, Nano Lett. **10**, 3209 (2010).

[8]J. C. Meyer, A. Chuvilin, G. Algara-Siller, J. Biskupek, and U. Kaiser, Nano Lett. **9**, 2683 (2009).

[9]G. Giovannetti, P. A. Khomyakov, G. Brocks, P. J. Kelly, and J. van den Brink, Phys. Rev. B **76**, 073103 (2007).

[10]D. Golberg, Y. Bando, Y. Huang, T. Terao, M. Mitome, C. Tang, and C. Zhi, ACSNANO **4**, 2979 (2010).

[11]S. Azevedo, J. R. Kaschny, C. M. C. de Castilho, and F. de Brito Mota, Eur. Phys. J. B **67**, 507 (2009).

[12]C. Jin, F. Lin, K. Suenaga, and S. Iijima, Phys. Rev. Lett. **102**, 195505 (2009).

[13]S. Azevedo, J. R. Kaschny, C. M. C de Castilho, and F. de Brito Mota, Nanotechnology **18**, 495707 (2007).

[14]G. Kresse, and J. Hafner Phys. Rev. B **47**, 558 (1993).

[15]G. Kresse, and J. Hafner Phys. Rev. B **49**, 14251 (1994).

[16]G. Kresse, and J. Furthmuller, Phys. Rev. B **54**, 11169 (1996).

[17]G. Kresse, and J. Furthmuller, Comput. Mater. Sci. **6**, 11169 (1996).

[18]J. P. Perdew, K. Burke, and M. Ernzerhof, Phys. Rev. Lett. **77**, 18 (1996).

[19]X. Hua, X. Chen, and W. A. Goddard, Phys. Rev. B **55**, 16103 (1997).

[20]A. Marini, G. Onida, and R. D. Sole, Phys. Rev. Lett. 88, 016403 (2001).

[21]F. Aryasetiawan, and O. Gunnarson, Rep. Prog. Phys. **61**, (1998) 237.

[22]G. Kresse, and J. Joubert, Phys. Rev. B **59**, 1758 (1999).

[23]P. E. Blöchl, Phys. Rev. B **50**, 17953 (1994).

[24]H. J. Monkhorst, and J. D. Pack, Phys. Rev. B **13**, 5188 (1976).

[25]J. Li, G. Gui, and J. Zhong, J. App. Phys. **104**, 094311 (2008).

[26]J. Neugebauer, and M. Scheffler, Phys. Rev. B **46**, 16 067 (1992).

[27]V. L Solozenko, G. Will, and F. Elf, Solid State Commun. **96**, 1 (1995).

[28]C. Attaccalite, M. Bockstedte, A. Marini, A. Rubio, and L. Wirtz, Phys. Rev. B **83**, 144115 (2011).

[29]H. Jónsson, G. Mills, and K. W. Jacobsen, *Nudged elastic band method for finding minimum energy paths of transitions*, in Classical and Quantum Dynamics in Condensed Phase Simulations, edited by B. J. Berne, G. Ciccotti, and D. F. Coker (World Scientific, Singapore, 1998), pp. 385.

[30]G. Mills, and H. Jónsson, Phys. Rev. Lett. **72**, 1124 (1994).

[31]G. Henkelman and H. Jónsson, J. Chem. Phys. **113**, 9978 (2000).

[32]S. B. Zhang, and J. E. Northrup, Phys. Rev. Lett. **67**, 2339 (1991).

[33]S. S. Wise, J. L. Margrave, H. M. Feder, and W. N. Hubbard, J. Phys. Chem. **70**, 7 (1966).

[34]I. Jiménez, A. Jankowski, L. J Terminello, J. A. Carlisle, D. G. J. Sutherland, G. L. Dol, J. L. Mantese, V. M. Tong, D. K. Shuh, and F. J. Himpsel, Appl. Phys. Lett. **68**, 2816 (1996).

[35]I. Jiménez, A. Jankowski, L. J. Terminello, D. G. J. Sutherland, J. A. Carlisle, G. L. Doll, V. M. Ton, D. Shuh, and F. J. Himpsel, Phys. Rev. B **55**, 12025 (1997).

[36]M. Topsakal, E. Aktürk, and S. Ciraci, Phys. Rev. B. **79**, 115442 (2009).

[37]J. Robles, and L. J. Bartolotti, J. Am. Chem. Soc., **106**, 3723 (1984).

[38]W. R. L. Lambrecht, and B. Segal, *Band structure of pure BN*, in Properties of Group-III Nitrides, edited by J. H. Edgar, EMIS Data Reviews Series (INSPEC Publications, London, 1994), pp. 129.

[39]E. D. Jones, N. A. Modine, A. A. Allerman, S. R. Kurtz, A. F. Wright, S. T. Tozer, and X. Wei, Phys. Rev. B **60**, 4430 (1999).

[40]R. J. Turton, *Calculational methods for determining the band structure of bulk c-Si*, in Properties of crystalline silicon, edited by R. Hull, EMIS Data Review Series, (INSPEC Publications, London, 1999), pp. 387.

[41]P. Schröer, P. Kruger, and J. Pollman, Phys. Rev. B. **47**, 6971 (1993); *ibid*. **48**, 18264 (1993).

[42]S. S. Alexandre, H. Chacham, and R. W. Nunes, Phys. Rev. B **63,** 125205 (2001).

[43]W. Orellana, and H. Chacham, Phys. Rev. B. **63**, 125205 (2001).

[44]W. Orellana, and H. Chacham, Appl. Phys. Lett. **74**, 2984 (1999).

[45]Z. Rak, S. D. Mahanti, K. C. Mandal, and N. C. Fernelius, Proc. MRS, 0994-F03-10 (2007).

[46]Z. Rak, S. D. Mahanti, K.C. Mandal, and N. C. Fernelius, J. Phys. Condens. Matter **21**, 015505 (2009).

[47]T. M. Schmidt, R. J. Baierle, P. Piquini, and A. Fazzio, Phys. Rev. B. **67**, 113407 (2003).

[48]W. Orellana, and H. Chacham, Phys. Rev. B. **62**, 10135 (2000).

[49]X. Blase, A. Rubio, S. G. Louie, and M. L. Cohen, Europhys. Lett. **28,** 335 (1994).

[50]G. Cappellini, G. Satta, M. Palummo, and G. Onida, Phys. Rev. B **64**, 035104 (2001).

[51]L. Museur, E. Feldbach, and A. Kanaev, Phys. Rev. B **78**, 155204 (2008).

[52]C. Zhi, Y. Bando, C. Tang, D. Golberg, Z. Xie, and T. Sekiguchi, Appl. Phys. Lett. **86**, 213110 (2005).

[53]J. Wu, W.-Q. Han, W. Walukiewicz, J. W. Ager III, W. Shan, E. E. Haller, and A. Zettl, Nano Lett. **4**, 647 (2004).

[54]P. Jaffrennou, J. Barjon, T. Schmid, L. Museur, A. Kanaev, J. -S. Lauret, C. Y. Zhi, C. Tang, Y. Bando, D. Golberg, B. Attal-Tretout, F. Ducastelle, and A. Loiseau, Phys. Rev. B **77**, 235422 (2008).

[55]M. G. Silly, P. Jaffrennou, J. Barjon, J. -S. Lauret, F. Ducastelle, A. Loiseau, E. Obraztsova, B. Attal-Tretout, and E. Rosencher, Phys. Rev. B **75**, 085205 (2007).

[56]G. Onida, L. Reining, and A. Rubio, Rev. Mod. Phys. **74**, 601 (2002).

[57]M. Bockstedte, A. Marini, O. Pankratov, and A. Rubio, Phys. Rev. Lett. **105**, 026401 (2010).

[58]Y. Ma, and M. Rohlfing, Phys. Rev. B **77**, 115118 (2008).

[59]K. Watanabe, T. Taniguchi, and H. Kanda, Nature Materials **3**, 404 (2004).

[60]W. J. Zhang, H. Kanda, and S. Matsumoto, Appl. Phys. Lett. **81**, 3356 (2002).

[61]C. A. Taylor II, S. W. Brown, V. Subramaniam, S. Kidner, S. C. Rand, and R. Clark, Appl. Phys. Lett. **65**, 1251 (1994).

[62]V. L. Solozhenko, A. G. Lazarenko, J. P. Petitet, and A. V. Kanaev, J. Phys. Chem. Solids **62**, 1331 (2001).

[63]B. Arnaud, S. Lebègue, P. Rabiller, and M. Alouani, Phys. Rev. Lett. **96**, 026402 (2006).

[64]L. Museur, and A. Kanaev, J. Appl. Phys. **103**, 103520 (2008).

[65]L. Wirtz, A. Marini, M. Gruning, C. Attaccalite, G. Kresse, and A. Rubio, Phys. Rev. Lett. **100**, 189701 (2008).

[66]K. Watanabe, and T. Taniguchi, Phys. Rev. B **79**, 193104 (2009).